

# ornl

**OAK RIDGE  
NATIONAL  
LABORATORY**

**MARTIN MARIETTA**

OPERATED BY  
MARTIN MARIETTA ENERGY SYSTEMS, INC.  
FOR THE UNITED STATES  
DEPARTMENT OF ENERGY



3 4456 0167510 4

ORNL/TM-9925

## Plasma Transport Coefficients for Nonsymmetric Toroidal Confinement Systems

S. P. Hirshman  
K. C. Shaing  
W. I. van Rij  
C. O. Beasley, Jr.  
E. C. Crume, Jr.

OAK RIDGE NATIONAL LABORATORY  
CENTRAL RESEARCH LIBRARY  
CIRCULATION SECTION  
EASTON ROOM 115  
**LIBRARY LOAN COPY**  
DO NOT TRANSFER TO ANOTHER PERSON  
If you wish someone else to see this  
report, send in name with report and  
the library will arrange a loan.

Printed in the United States of America. Available from  
National Technical Information Service  
U.S. Department of Commerce  
5285 Port Royal Road, Springfield, Virginia 22161  
NTIS price codes—Printed Copy: A03; Microfiche A01

This report was prepared as an account of work sponsored by an agency of the United States Government. Neither the United States Government nor any agency thereof, nor any of their employees, makes any warranty, express or implied, or assumes any legal liability or responsibility for the accuracy, completeness, or usefulness of any information, apparatus, product, or process disclosed, or represents that its use would not infringe privately owned rights. Reference herein to any specific commercial product, process, or service by trade name, trademark, manufacturer, or otherwise, does not necessarily constitute or imply its endorsement, recommendation, or favoring by the United States Government or any agency thereof. The views and opinions of authors expressed herein do not necessarily state or reflect those of the United States Government or any agency thereof.

Fusion Energy Division

PLASMA TRANSPORT COEFFICIENTS  
FOR NONSYMMETRIC TOROIDAL CONFINEMENT SYSTEMS

S. P. Hirshman  
K. C. Shaing  
W. I. van Rij  
C. O. Beasley, Jr.  
E. C. Crume, Jr.

Date Published - March 1986

**NOTICE** This document contains information of a preliminary nature.  
It is subject to revision or correction and therefore does not represent a  
final report.

Prepared by the  
OAK RIDGE NATIONAL LABORATORY  
Oak Ridge, Tennessee 37831  
operated by  
MARTIN MARIETTA ENERGY SYSTEMS, INC.  
for the  
U. S. DEPARTMENT OF ENERGY  
under Contract No. DE-AC05-84OR21400



3 4456 0167510 4



## CONTENTS

ABSTRACT.....	v
I. INTRODUCTION.....	1
II. BASIC EQUATIONS AND TRANSPORT ORDERINGS.....	5
III. VARIATIONAL PRINCIPLE.....	10
IV. FOURIER-LEGENDRE EXPANSION OF THE DISTRIBUTION FUNCTION.....	14
V. NUMERICAL METHOD.....	18
VI. NUMERICAL RESULTS.....	20
VII. CONCLUSIONS.....	32
ACKNOWLEDGMENTS.....	32
REFERENCES.....	33



## ABSTRACT

A variational principle is developed for computing accurate values of local plasma transport coefficients in nonsymmetric toroidal confinement configurations. Numerical solutions of the linearized drift Fokker-Planck equation are used to obtain the thermodynamic fluxes as functions of collision frequency and the radial electric field. Effects resulting from the variation of the longitudinal adiabatic invariant  $J$  along an orbit (due to particle transitions from helically trapped to toroidally trapped orbits) are treated. The velocity-space distribution resulting from trapped, circulating, and transition particle orbits is well represented by a Legendre polynomial expansion in the pitch angle coordinate. The computational effort is significantly reduced from that required with Monte Carlo methods through use of an efficient treatment of the disparity between the time scales of collisionless and collisional particle dynamics. Numerical computations for a stellarator configuration are presented.



## I. INTRODUCTION

The numerical computation of transport coefficients for three-dimensional (3-D) plasma configurations is motivated by the need to avoid the numerous asymptotic approximations required for any tractable analytic theory. These approximations are generally of two kinds: (1) model magnetic fields and (2) multiple-time-scale expansions. Model field approximations include a large-aspect-ratio expansion for the magnetic field strength  $B \equiv |\vec{B}|$ , the assumption of a small rotational transform  $\iota$  per field period  $N$  (which permits bounce-averaging trapped orbits without encountering angle periodicity problems), and the neglect of finite  $\epsilon_h/\epsilon_t$  and pressure effects on  $B$  and the consequent modification of particle orbits. Here  $\epsilon_h$  ( $\epsilon_t$ ) is the helical (poloidal) modulation of  $B$ . Multiple-time-scale expansions are used to obtain asymptotic expansions of the kinetic equation in various collision frequency regimes characterized by different values of collisionality  $\nu_* \equiv \nu_{\text{eff}}/\omega_b$ , where  $\nu_{\text{eff}}$  is the effective collision frequency and  $\omega_b$  is the bounce frequency of a particular class of trapped particles. Obtaining continuous distribution functions for distinct classes of trapped and circulating particles (which often exhibit different values of  $\nu_*$ ) is difficult, and the neglect of different terms in the analytic theory can lead to flux discrepancies that are not easily resolved.<sup>1-3</sup>

Using numerical methods, the effects of finite plasma pressure and toroidal aspect ratio on transport can be assessed without resorting to magnetic field models. This is particularly significant for coil and reactor optimization studies. As an example, transport in Helic configurations with  $\iota/N \sim 0.5$ , for which no simple analytic form for

the second adiabatic invariant  $J$  exists, can only be treated numerically.

The relaxation of the multiple-time-scale approximations enables computation of the transport associated with all classes of trapped and circulating particles over a wide range of  $v_*$ . In particular, the transport arising from transition particles, for which the longitudinal invariant  $J$  is not a conserved quantity, may be accurately assessed. The resulting distribution function  $f(\vec{x}, \vec{v})$  is a continuous function of velocity-space coordinates for all values of  $v_*$ . This is in contrast to the boundary layers that develop when, in a Fokker-Planck code, bounce-averaged approximate orbits are used for helically trapped particles.<sup>4</sup> The inclusion of "collisionless-detrapping"<sup>1</sup> particle dynamics thus yields natural boundary conditions between regions of phase space with different orbit topologies; a transport flux results that is a continuous and unique function of the collision frequency.

Matching the particle distributions across trapped and circulating portions of phase space can be accomplished by using a form of the drift kinetic equation that includes transition particles, which are characterized by  $dJ/dt \neq 0$ . For these particles, retention of only the bounce-averaged portion of their orbits does not adequately describe their motion. The inclusion of transition particle physics significantly complicates the phase space, and hence the solution, for the particle distribution function  $f$ . However, this complexity is offset by the additional physics present in the nonlocal solution for  $f$ . For example, when  $\vec{B} \cdot \nabla f = 0$  (the derivative is taken with the energy and magnetic moment held constant), the parallel viscous stress rigorously vanishes.<sup>5</sup> Thus, the bootstrap current (which is of particular

importance in stellarators without Ohmic currents), as well as contributions to the radial transport in the plateau<sup>6</sup> and Pfirsch-Schlüter<sup>7</sup> regimes arising from the helical modulation of the magnetic field, can be evaluated only from the nonlocal distribution function.

The disparity between the time scales of the rapid bounce motion of trapped particles, collisional scattering, and the much slower magnetic drifts causes the main numerical problems in computing the nonlocal distribution function. For example, in Monte Carlo numerical simulations,<sup>8,9</sup> single particle orbits must be integrated for at least several collision times, during which many bounces in the helical magnetic wells will occur. Since the numerically stable time step is set by this rapid bounce motion, many thousands of iterations may be needed to determine the diffusive step size in the long mean-free-path regimes. Recent Monte Carlo calculations using only the bounce-averaged orbit dynamics are therefore much more efficient than corresponding full orbit simulations.<sup>10</sup> However, the relatively crude statistics of Monte Carlo results that can be obtained in reasonable amounts of computer time make detailed comparisons with analytic theories difficult. In addition, the presence of loss-cone orbits may further obscure the comparison.

The numerical solution of the drift kinetic equation also reflects this time-scale disparity through the eigenvalue structure of the linearized drift Fokker-Planck propagator. In the low-collision-frequency regime of interest,  $\nu_* \ll 1$ , the eigenvalues  $\lambda$  of this propagator are nearly imaginary,  $\lambda/\omega_b \sim -\nu_* + i$ , corresponding to underdamped bounce motion. For a stable time step  $\Delta t \sim \omega_b^{-1}$ , a

steady-state solution will be reached only after  $(\omega_b \Delta t v_*)^{-1} \gg 1$  iterations of the kinetic equation.

It is therefore apparent that following the true temporal evolution of particle orbits, either with Monte Carlo methods or with kinetic equations,<sup>11</sup> is an extremely inefficient way to obtain the steady-state distribution function, and hence the transport coefficients, in the low-collision-frequency regime. Two alternative solution methods are discussed in this paper. One numerical scheme accelerates convergence to the stationary state by rotating the eigenvalues of the drift propagator in the complex plane to produce strong damping. This method sacrifices information about the true temporal behavior of the distribution for speed. Another solution method inverts the block-tridiagonal steady-state equations. In the low-collision-frequency regime, this method is generally faster than the accelerated temporal integration scheme but requires more storage.

This paper is organized as follows. A conservative form for the linearized drift kinetic equation is derived in Sec. II for a straight magnetic field line flux coordinate representation. A variational principle for the transport coefficients, valid for arbitrary collision frequencies and not requiring piecewise J conservation, is obtained in Sec. III. In Sec. IV, the Fourier-Legendre expansion for the spatial and pitch angle dependence of the distribution function is introduced, and the resulting representation for the kinetic equation is obtained. Efficient numerical methods for solving the drift equation in the low-collision-frequency regime are discussed in Sec. V. In Sec. VI, computations for a stellarator configuration are presented, and it is shown that transport can be strongly affected by resonances and

transition particle orbits in systems with finite values of  $1/N$ , compared to systems with well-defined local helical wells ( $N \rightarrow \infty$ ).

## II. BASIC EQUATIONS AND TRANSPORT ORDERINGS

The evolution of the particle distribution function  $f(\vec{x}, \vec{v}, t)$  in the presence of multiple small-angle collisions is governed by the Fokker-Planck equation. The velocity  $\vec{v} = v_{\parallel} \vec{n} + v_{\perp} (\cos \phi \vec{e}_1 + \sin \phi \vec{e}_2)$ , where  $(\vec{n} = \vec{B}/B, \vec{e}_1, \vec{e}_2)$  form a local orthogonal coordinate system aligned with the magnetic field. Expanding in powers of  $B^{-1}$  yields the following reduced (or drift kinetic) equation<sup>1,2</sup> for the part of  $f$  independent of the gyrophase angle  $\phi$ :

$$\frac{\partial f}{\partial t} + \vec{v}_g \cdot \frac{\partial f}{\partial \vec{x}} + \vec{a}_g \cdot \frac{\partial f}{\partial \vec{v}} = C(f, f) \quad (1)$$

Here,  $\vec{v}_g = (v_{\parallel} + u) \vec{n} + \vec{v}_D$  is the guiding center velocity, where  $v_{\parallel} = \vec{n} \cdot \vec{v}$  and  $u = v_{\perp}^2 / (2\Omega) \vec{n} \cdot \nabla \times \vec{n}$  is the first-order correction (in  $B^{-1}$ ) to the parallel speed;  $v_{\perp} = (v^2 - v_{\parallel}^2)^{1/2}$  is the perpendicular speed;  $\Omega = eB/m$  is the gyrofrequency; and

$$\vec{v}_D = \frac{\vec{F}_g \times \vec{n}}{m\Omega} + \left[ \nabla \times \vec{n} - (\vec{n} \cdot \nabla \times \vec{n}) \vec{n} \right] \frac{v_{\parallel}^2}{\Omega} \quad (2)$$

is the guiding center drift across the magnetic field, where  $\vec{F}_g = e\vec{E} - (mv_{\perp}^2/2)\nabla \ln B$ .

The spherical velocity-space coordinates  $(v, \alpha, \phi)$ , where  $v_{\parallel} = v \cos \alpha$  and  $\alpha$  is the pitch angle, are convenient for numerical computations,<sup>13</sup> since their range of definition is independent of the real-space position  $\vec{x}$ . (This is in contrast to the analytically favored adiabatic invariants  $\mu$  and  $\varepsilon$ , which couple real space and velocity space in a manner difficult to treat numerically.) In addition, the linearized collision term has a simple representation in these coordinates. Then, the spherical velocity-space representation of the guiding center acceleration term in Eq. (1) is:

$$\vec{a}_g \cdot \frac{\partial f}{\partial \vec{v}} = \dot{\alpha} \frac{\partial f}{\partial \alpha} + \dot{v} \frac{\partial f}{\partial v} , \quad (3)$$

where

$$\dot{\alpha} = - \frac{\sin \alpha}{mv} \vec{n} \cdot \vec{F}_g + \frac{1}{2} \sin \alpha \cos \alpha A_{\alpha} , \quad (4a)$$

$$\dot{v} = \frac{e}{mv} \vec{E} \cdot \vec{v}_g , \quad (4b)$$

$$A_{\alpha} = \frac{3(\vec{n} \cdot \nabla \times \vec{n})}{m\Omega} \vec{n} \cdot \vec{F}_g - \frac{2\nabla \times \vec{n}}{m\Omega} \cdot \vec{F}_g + \vec{v}_g \cdot \nabla \ln B + \frac{v^2}{\Omega} \vec{B} \cdot \nabla \left( \frac{\vec{n} \cdot \nabla \times \vec{n}}{B} \right) . \quad (4c)$$

For the quasi-static magnetic field configurations of interest in transport applications ( $\partial B / \partial t \approx 0$  on the collisional time scale), Eq. (1) has the following conservative form:<sup>14</sup>

$$\frac{\partial f}{\partial t} + \nabla \cdot (\vec{v}_g f) + \frac{1}{\sin \alpha} \frac{\partial}{\partial \alpha} (\sin \alpha \dot{\alpha} f) + \frac{1}{v^2} \frac{\partial}{\partial v} (v^2 \dot{v} f) = C(f, f) . \quad (5)$$

The conservative form of Eq. (1) given by Eq. (5) is useful in establishing variational properties of the drift kinetic equation.

For transport calculations, Eq. (1) may be expanded about a local Maxwellian  $f_M$  as follows:

$$f = f_M \left[ 1 + \frac{e}{T} \int^l \left( \frac{\vec{E} \cdot \vec{B}}{B^2} - \frac{\langle \vec{E} \cdot \vec{B} \rangle}{\langle E^2 \rangle} \right) B dl' \right] + f_1 , \quad (6a)$$

$$f_M = \frac{n}{(\pi^{1/2} v_T)^3} \exp(-K) , \quad (6b)$$

where  $v_T = (2T/m)^{1/2}$  is the local thermal velocity,  $K = mv^2/(2T)$  is the normalized kinetic energy, and  $f_1$  is the perturbation due to small local departures from thermodynamic equilibrium. In Eq. (6), the density  $n = n(\rho)$  and the temperature  $T = T(\rho)$  are constant on the magnetic flux surface labeled by  $\rho = \text{const}$ . Here, spatial flux coordinates  $(\rho, \theta, \zeta)$  are defined through the magnetic mapping equations<sup>15</sup>  $(R, \phi, Z) \rightarrow (\rho, \theta, \zeta)$ . They are obtained by solving the MHD force equilibrium equation  $\vec{J} \times \vec{B} = \nabla p$ , with  $\mu_0 \vec{J} = \nabla \times \vec{B}$  and

$$\vec{B} = -\chi' \nabla \rho \times \nabla \zeta + \psi' \nabla \rho \times \nabla \theta . \quad (7)$$

The poloidal and toroidal magnetic fluxes in Eq. (7) are  $2\pi\chi(\rho)$  and  $2\pi\psi(\rho)$ , respectively, with the prime denoting  $\partial/\partial\rho$ . The rotational

transform is  $\iota = \chi' / \psi'$ , and the flux-surface-average operator [indicated by the angle brackets in Eq. (6)] is defined as

$$\langle A \rangle = \frac{\int \int \sqrt{g} A \, d\theta \, d\zeta}{\int \int \sqrt{g} \, d\theta \, d\zeta} . \quad (8)$$

Here,  $\sqrt{g} = (\nabla\rho \cdot \nabla\theta \times \nabla\zeta)^{-1}$  is the real-space Jacobian.

Inserting Eq. (6a) into Eq. (1) and using the form for  $\vec{B}$  given by Eq. (7) yields the following steady-state linear equation for  $f_1$ :

$$\vec{v}_L \cdot \nabla f_1 + \dot{\alpha}_L \frac{\partial f_1}{\partial \alpha} + \dot{v}_L \frac{\partial f_1}{\partial v} - C(f_1) = D , \quad (9)$$

where

$$\vec{v}_L = v \cos \alpha \vec{n} + E_\rho \frac{\nabla\rho \times \vec{n}}{B} , \quad (10a)$$

$$\dot{\alpha}_L = -\frac{1}{2} v \sin \alpha \vec{B} \cdot \nabla \frac{1}{B} - \frac{1}{2} \frac{E_\rho}{B} \nabla\rho \cdot \nabla \times \vec{n} \sin \alpha \cos \alpha , \quad (10b)$$

$$\dot{v}_L = \frac{E_\rho v}{4B} (3 + \cos 2\alpha) \nabla\rho \cdot \nabla \times \vec{n} , \quad (10c)$$

$$D = \left[ -\vec{v}_D \cdot \nabla\rho (A_1 + KA_2) - Bv \cos \alpha A_3 \right] f_M , \quad (10d)$$

$$A_1 = \frac{n'}{n} - \frac{3}{2} \frac{T'}{T} - \frac{eE_\rho}{T} , \quad (10e)$$

$$A_2 = \frac{T'}{T} , \quad (10f)$$

$$A_3 = \frac{-e}{T} \frac{\langle \vec{E} \cdot \vec{B} \rangle}{\langle B^2 \rangle} . \quad (10g)$$

The equilibrium relation  $\vec{J} \cdot \nabla \rho = 0 = \nabla \times \vec{B} \cdot \nabla \rho$  has been used to eliminate  $\nabla \rho \cdot \vec{n} \times \nabla \ln B = \nabla \rho \cdot \nabla \times \vec{n}$  from Eq. (10). Terms of order  $1/B$  have been neglected in  $\vec{v}_L$  and  $\dot{\alpha}_L$ , but the electric field drift due to  $\vec{E}_0 = \nabla \rho E_\rho$ , where  $E_\rho = -d\phi_0/d\rho$ , has been retained to account for the precession of deeply trapped particles with  $\cos \alpha = 0$ . (The neglect of the remaining order  $1/B$  terms in  $\vec{v}_D \cdot \nabla f_1$  precludes the study of resonant superbanana<sup>16</sup> orbits in the present formulation.) The inclusion of the terms  $\sim E_\rho$  in  $\dot{\alpha}_L$  and  $\dot{v}_L$  ensures that Eq. (5), with  $\vec{v}_g = \vec{v}_L$ ,  $\dot{\alpha} = \dot{\alpha}_L$ , and  $\dot{v} = \dot{v}_L$ , is satisfied. Thus, Eq. (9) is conservative.

The precession of helically trapped particles due to the radial electric field  $E_\rho$  can be treated approximately by neglecting the terms proportional to  $E_\rho \nabla \rho \cdot \nabla \times \vec{n}$  in  $\dot{\alpha}_L$  and  $\dot{v}_L$ . Since  $\nabla \rho \cdot \nabla \times \vec{n} = \vec{B} \times \nabla \rho \cdot \nabla B^{-1}$ , this approximation discards terms of order  $\delta B(E_\rho)$ , the product of the modulation of  $B$  (denoted  $\delta B$ ) and the radial electric field. The primary advantage afforded by this approximation is the elimination of the  $v$  derivative from Eq. (9). To retain the conservative property of Eq. (9), Eq. (10a) is written  $\vec{v}_L = v \cos \alpha \vec{n} + \vec{v}_E$ , where  $\vec{v}_E = E_\rho \nabla \rho \times \vec{B} / \langle B^2 \rangle$  is incompressible:  $\nabla \cdot \vec{v}_E = 0$ . The resulting difference in  $\vec{v}_L$  is of order  $\delta B(E_\rho)$ .

In magnetic flux coordinates, the parallel gradient operator is

$$\vec{B} \cdot \nabla = \frac{X'}{\sqrt{g}} \frac{\partial}{\partial \theta} + \frac{\psi'}{\sqrt{g}} \frac{\partial}{\partial \zeta}, \quad (11)$$

and the radial component of the drift velocity becomes

$$\vec{v}_D \cdot \nabla \rho = \frac{v^2}{3} \frac{B}{\Omega} \left[ 1 + \frac{1}{2} P_2(\cos \alpha) \right] s(\vec{x}) \quad , \quad (12a)$$

$$s(\vec{x}) = \frac{1}{\sqrt{g}} \left[ \frac{\partial}{\partial \theta} \left( \frac{B_\zeta}{B^2} \right) - \frac{\partial}{\partial \zeta} \left( \frac{B_\theta}{B^2} \right) \right] \quad , \quad (12b)$$

where  $P_2$  is the Legendre polynomial of order 2. In Eq. (12b),  $B_\theta$  and  $B_\zeta$  are the covariant components of  $\vec{B}$ , which, by virtue of  $\vec{J} \cdot \nabla \rho = 0$ , satisfy

$$\frac{\partial B_\theta}{\partial \zeta} - \frac{\partial B_\zeta}{\partial \theta} = 0 \quad . \quad (12c)$$

In the axisymmetric limit,  $B_\zeta = RB_T = F(\rho)$ .

### III. VARIATIONAL PRINCIPLE

A variational principle for the thermodynamic fluxes is now derived from the linearized equation, Eq. (9), with  $\dot{v}_L = 0$ . Various limiting variational forms have been previously obtained, corresponding to both very low collisionality<sup>16</sup> [for which a bounce-averaged version of Eq. (9) was used] and the higher-collisionality  $1/\nu$  regime.<sup>17</sup> Since the present investigation attempts to include transition particle dynamics (for which previous expansions are inappropriate), a variational principle is required that is valid for all collisionalities.

It is convenient to recast Eq. (9) as follows:

$$\hat{V}(g_1) - \hat{C}(g_1) = D, \quad (13)$$

where  $g_1 \equiv f_1/f_M$  is the perturbed distribution with the Maxwellian factored out,  $\hat{V}(g_1) \equiv f_M V(g_1)$ , and  $\hat{C}(g_1) \equiv C(f_M g_1)$ . The relation  $V(f_M g_1) = f_M V(g_1)$  was used for the linearized Vlasov operator  $V \equiv \vec{v}_L \cdot \nabla + \dot{\alpha}_L \partial / \partial \alpha$ . This follows from  $V(f_M) = 0$  and the fact that  $V$  involves only first-order derivatives. Now define the inner product

$$\{f, h\} \equiv 2\pi \int d(\cos \alpha) \int \langle fh \rangle v^2 dv. \quad (14)$$

When energy scattering is ignored, the  $v^2 dv$  integral in Eq. (14) is optional. Noting that the linearized Vlasov equation can be written in conservative form [see Eq. (5)], it follows from integration by parts that  $\hat{V}$  is an antisymmetric operator with respect to the inner product:

$$\{f, \hat{V}(h)\} = -\{h, \hat{V}(f)\}. \quad (15a)$$

Similarly,  $\hat{C}$  is a symmetric operator:

$$\{f, \hat{C}(h)\} = \{h, \hat{C}(f)\}. \quad (15b)$$

Thus, the total linearized operator in Eq. (9) has no definite symmetry structure with respect to the inner product. To obtain a variational principle for such an equation, it is necessary to introduce the adjoint equation:

$$-\hat{V}(h_1) - \hat{C}(h_1) = D^*. \quad (16)$$

When  $D^*$  is chosen to satisfy  $D^*(E_{||}, \alpha) \equiv D(-E_{||}, \pi - \alpha) = D(E_{||}, \alpha)$ , the solution  $h_1$  of Eq. (16) is related to  $g_1$  in Eq. (13), for fixed  $A_1$  and  $A_2$ , as follows:

$$h_1(E_\rho, E_{||}, \alpha) = g_1(-E_\rho, -E_{||}, \pi - \alpha) . \quad (17)$$

Equation (17) expresses the fact that the adjoint equation has reversed orbits,  $E_\rho \rightarrow -E_\rho$ , and  $E_{||} \rightarrow -E_{||}$ ,  $v_{||} \rightarrow -v_{||}$ , compared with Eq. (13).

To obtain equations with definite symmetry properties, the sum and difference distributions,  $F^\pm$ , are introduced:

$$F^\pm \equiv \frac{1}{2}(g_1 \pm h_1) . \quad (18)$$

Adding and subtracting Eqs. (13) and (16) with  $D^* = D$  yields

$$\hat{V}(F^-) - \hat{C}(F^+) = D , \quad (19a)$$

$$\hat{V}(F^+) - \hat{C}(F^-) = 0 . \quad (19b)$$

Equation (19) is now suitable for deriving a variational form. Multiplying Eq. (19a) by  $F^+$  and Eq. (19b) by  $F^-$  and taking the inner product of the difference yields

$$\dot{S}_0 = 2\{F^+, \hat{V}(F^-)\} - \{F^+, \hat{C}(F^+)\} + \{F^-, \hat{C}(F^-)\} - \{F^+, D\} . \quad (20a)$$

By construction,  $\dot{S}_0$  vanishes when  $F^\pm$  satisfy Eq. (19). Then, the entropy production rate  $\dot{S} \equiv \dot{S}_0 - \{F^+, D\}$  is

$$\dot{S} = 2\{F^+, \hat{V}(F^-)\} - \{F^+, \hat{C}(F^+)\} + \{F^-, \hat{C}(F^-)\} - 2\{F^+, D\} . \quad (20b)$$

Using the symmetry properties of  $\hat{V}$  and  $\hat{C}$  given by Eq. (15), it follows that  $\dot{S}$  is a variational quantity with respect to  $F^\pm$  and attains its stationary value,  $\dot{S}_* = -\{F^+, D\}$ , when  $F^\pm$  satisfy Eq. (19). Multiplying Eq. (13) by  $h_1$  and Eq. (16) by  $g_1$  and subtracting yields  $\{g_1, D\} = \{h_1, D\}$ , or  $\{F^-, D\} = 0$ . Thus,

$$\dot{S}_* = -\{g_1, D\} = \sum_{j=1}^3 I_j A_j, \quad (21)$$

where  $I_j$  are the thermodynamic fluxes conjugate to the forces  $A_j$ :

$$I_1 \equiv \langle \vec{\Gamma} \cdot \nabla \rho \rangle = - \sum_{n=1}^3 L_{1n} A_n, \quad (22a)$$

$$I_2 \equiv \left\langle \frac{\vec{Q} \cdot \nabla \rho}{T} \right\rangle = - \sum_{n=1}^3 L_{2n} A_n, \quad (22b)$$

$$I_3 \equiv n \langle \vec{u} \cdot \vec{B} \rangle = - \sum_{n=1}^3 L_{3n} A_n. \quad (22c)$$

Here,  $\vec{\Gamma} = \int v_D \vec{f}_1 d^3v$  is the particle flux,  $\vec{Q} = T \int v_D K \vec{f}_1 d^3v$  is the heat flux, and  $n \vec{u} \cdot \vec{B} = B \int v_{\parallel} \vec{f}_1 d^3v$ .

The coefficients  $L_{ij}$  defined in Eq. (22) are elements of the Onsager transport matrix. The relations  $\delta S / \delta F^\pm = 0$  together with Eq. (21) make up a variational principle for computing accurate values for these transport matrix elements in all collision frequency regimes. (The constancy of the longitudinal adiabatic invariant  $J$  is not required for the validity of this result.) The derivation of Eqs. (20) and (21) can be generalized to prove that the transport matrix is symmetric and positive definite, namely,  $L_{ij} = L_{ji}$  and  $\dot{S}_* \leq 0$ , with  $\dot{S}_* = 0$  only if  $A_i = 0$  for  $i = 1-3$ .

Since  $\hat{C}$  is a negative operator, its inverse is well defined except for functions comprising the collisional invariants (which are in the null space of  $\hat{C}$ ). It is computationally efficient to consider the augmented negative definite operator,  $\hat{C}_\varepsilon = \hat{C} + \varepsilon$ , where  $\varepsilon \rightarrow 0^-$  has negative eigenvalues in the null space of  $\hat{C}$ . The operator  $\hat{C}_\varepsilon$  is rigorously invertible, and the transport coefficients can be computed as the limit of a sequence corresponding to decreasing values of  $\varepsilon$ . (In practice,  $\varepsilon$  has only a weak effect on the transport coefficients.) Thus,

$$F^- = \hat{C}_\varepsilon^{-1} \hat{V}(F^+) \quad , \quad (23a)$$

and substituting this into the expression for  $\dot{S}$  yields the following quadratic form for  $F^+$ :

$$\dot{S}(F^+) = \lim_{\varepsilon \rightarrow 0^-} \left[ \left\{ F^+, \hat{V} \hat{C}_\varepsilon^{-1} \hat{V}(F^+) \right\} - \left\{ F^+, \hat{C}(F^+) \right\} - 2 \left\{ F^+, D \right\} \right] \quad . \quad (23b)$$

Since the operator  $\hat{V} \hat{C}_\varepsilon^{-1} \hat{V} - \hat{C}$  is positive definite, the extremal value of  $\dot{S}$  obtained by varying with respect to  $F^+$  corresponds to a minimum. Equation (23b) is therefore an energy principle for determining the thermodynamic fluxes.

#### IV. FOURIER-LEGENDRE EXPANSION OF THE DISTRIBUTION FUNCTION

The variational distributions  $F^\pm$  defined in Eq. (18) may be expanded in a Fourier-Legendre series as follows:<sup>13</sup>

$$F^\pm = \sum_{i=1}^3 A_i \left\{ \sum_1 p_1(\cos \alpha) \sum_{m,n} \sum_{\gamma=c,s} F_{imnl}^{\pm\gamma}(v) e_{mn}^\gamma(\theta, \zeta) \right\} \quad . \quad (24)$$

Here,  $0 \leq l \leq L$  ( $L$  is the maximum order in a truncated Legendre series approximation for  $F^{\pm}$ ) and  $p_l(x) = (1 + 1/2)^{1/2} P_l(x)$  are the orthonormalized Legendre polynomials (with unity weight factor). The  $e_{mn}^Y(\theta, \zeta)$  are orthonormalized trigonometric functions for  $0 \leq m \leq M$  and  $-N \leq n \leq N$  (for  $m = 0$ ,  $0 \leq n \leq N$ ):  $e_{mn}^c = \sqrt{2} \cos(m\theta - n\zeta)$  for  $m$  or  $n$  nonzero,  $e_{00}^c = 1$ , and  $e_{mn}^s = \sqrt{2} \sin(m\theta - n\zeta)$ .

Henceforth, energy scattering will be neglected in the collision term in Eq. (19). Then, the velocity dependence of  $F^{\pm\gamma}$  may be explicitly factored as follows:

$$F_{imnl}^{\pm\gamma} = \begin{cases} \frac{vB}{\Omega} f_{1mnl}^{\pm\gamma}, & i = 1 \\ \frac{vB}{\Omega} K f_{2mnl}^{\pm\gamma}, & i = 2 \end{cases} \quad (25)$$

and  $F_{3mnl}^{\pm\gamma} = f_{3mnl}^{\pm\gamma}$ . Inserting this into Eq. (20b) or (23b) and varying with respect to the expansion coefficients  $f_{imnl}^{\pm\gamma}$  yields the  $\sqrt{g} p_l(\cos \alpha) e_{mn}^Y(\theta, \zeta)$  moments of Eq. (19). Restricting the present analysis to reflectionally symmetric magnetic fields that satisfy  $B(\theta, \zeta) = B(-\theta, -\zeta)$ , it follows that in Eq. (24), only  $F_{1mnl}^{+s} = F_{2mnl}^{+s}$ ,  $F_{1mnl}^{-c} = F_{2mnl}^{-c}$ ,  $F_{3mnl}^{+c}$ , and  $F_{3mnl}^{-s}$  are nonzero. The resulting variational equations for the expansion coefficients in Eq. (24) are (the  $\pm$  superscripts are subsequently suppressed, and summation over repeated primed subscripts is assumed):

$$A_{imnl}^c = - \left( Q_{ll'}^- \beta_{mn, m'n'}^s B_{mn, m'n'}^s - Q_{ll'}^+ \beta_{m'n', mn, m'n'}^c B_{mn, m'n'}^c \right) f_{im'n'l}^s - E_{mn, m'n'}^s f_{im'n'l}^s - v^{-1} g_{mn, m'n'}^c C_l \left( f_{im'n'l}^c \right) - D_{imnl}^c = 0, \quad (26a)$$

$$\begin{aligned}
A_{imnl}^S &\equiv \left( Q_{1l'}^- \beta_{mn} B^C_{mn,m'n'} - Q_{1l'}^+ \beta_{m'n'} B^S_{mn,m'n'} \right) f_{im'n'l'}^C \\
&+ E_{mn,m'n'}^C f_{im'n'l'}^C - v^{-1} g_{mn,m'n'}^S C_{l'}(f_{im'n'l'}^S) - D_{imnl}^S = 0 .
\end{aligned} \tag{26b}$$

$$\text{Here, } D_{1mnl}^C = D_{2mnl}^C = 0 = D_{3mnl}^S ,$$

$$Q_{1l'}^\pm = q_1^\pm \delta_{l' \pm 1, l'} - q_{l'}^\mp \delta_{l' \pm 1, l'} , \tag{27a}$$

$$q_1^\pm = 0.51(1 \pm 1) |4l^2 - 1|^{-1/2} , \tag{27b}$$

$$\beta_{mn} = m\chi' - n\psi' , \tag{27c}$$

$$B_{mn,m'n'}^Y = \langle\langle e_{mn}^Y(\theta, \zeta) \frac{1}{B} e_{m'n'}^Y(\theta, \zeta) \rangle\rangle , \tag{27d}$$

$$E_{mn,m'n'}^Y = \frac{E_p}{\langle B^2 \rangle_V} \langle\langle e_{mn}^Y(\theta, \zeta) (mB_\zeta + nB_\theta) e_{m'n'}^Y(\theta, \zeta) \rangle\rangle , \tag{27e}$$

$$g_{mn,m'n'}^Y = \langle\langle e_{mn}^Y(\theta, \zeta) \sqrt{g} e_{m'n'}^Y(\theta, \zeta) \rangle\rangle , \tag{27f}$$

$$D_{1mnl}^S = -\frac{1}{3} \langle\langle e_{mn}^S(\theta, \zeta) \sqrt{g} s(\vec{x}) \rangle\rangle \left( \sqrt{2} \delta_{10} + \frac{1}{\sqrt{10}} \delta_{12} \right) = D_{2mnl}^S , \tag{27g}$$

$$D_{3mnl}^C = -\langle\langle e_{mn}^C(\theta, \zeta) \sqrt{g} B \rangle\rangle \left( \frac{2}{3} \right)^{1/2} \delta_{11} , \tag{27h}$$

and  $\langle\langle A \rangle\rangle \equiv (2\pi)^{-2} \iint A d\theta d\zeta$ . In Eq. (26), the collision term is  $C_1(f_1) \equiv \int d(\cos \alpha) p_1(\cos \alpha) \hat{C}(f)$ .

Several special choices of flux coordinates lead to simplification of the matrix elements in Eq. (27). For Hamada coordinates,  $\sqrt{g} = \text{const}$ , and thus  $g^C = \sqrt{g} \delta_{mm'} \delta_{nn'}$ , and  $g^S = g^C(1 - \delta_{m0} \delta_{n0})$ . For Boozer coordinates,  $\sqrt{g} \sim B^{-2}$  and  $mB_\zeta + nB_\theta$  is independent of  $\theta$  and  $\zeta$ .

Then,  $E^S = E^C = v^{-1} [E_\rho (mB_\zeta + nB_\theta) / \langle B^2 \rangle] \delta_{mm'} \delta_{nn'}$ . In general, the relation

$$\sqrt{g} = \chi' \frac{B_\theta}{B^2} + \psi' \frac{B_\zeta}{B^2} \quad (28)$$

is used to eliminate  $\sqrt{g}$  from the matrix elements in Eq. (27).

In practice, Eq. (26) is solved for several different values of  $\hat{E} = E_\rho / v$  and  $\hat{v} = v(K) / v$  to obtain  $f_{imnl}^\gamma(\hat{E}, \hat{v})$ . The transport coefficients  $L_{ij}$  defined in Eq. (22) may be conveniently expressed in terms of the following normalized Fourier amplitudes of  $f$  and  $D$ :

$$\left( \hat{f}_{imnl}^\gamma, \hat{D}_{imnl}^\gamma \right) = \begin{cases} \frac{v_T B}{\Omega} K^{3/4} \left( f_{imnl}^\gamma, D_{imnl}^\gamma \right), & i \leq 2, \\ K^{1/4} \left( f_{3mnl}^\gamma, D_{3mnl}^\gamma \right), & i = 3. \end{cases} \quad (29)$$

Then,

$$L_{ij} = \frac{2}{\sqrt{\pi}} \int_0^\infty K^{1/2} e^{-K} g_i g_j D_{ij}(K) dK, \quad (30a)$$

where  $g_1 = g_3 = 1$ ,  $g_2 = K$ , and the velocity-dependent diffusion coefficient is

$$D_{ij}(K) = \frac{1}{2} \frac{nv_T}{V'} \sum_{\gamma=c,s} \sum_{m,n,l} \hat{D}_{imnl}^\gamma \hat{f}_{jmnl}^\gamma \left[ \frac{E_\rho}{v_T} K^{-1/2}, \frac{v(K)}{v_T} K^{-1/2} \right]. \quad (30b)$$

Here,  $V' \equiv \langle \langle \sqrt{g} \rangle \rangle$ . Note that for  $i \leq 2$  ( $i = 3$ ), only the sine (cosine) components,  $\gamma = s$  ( $\gamma = c$ ), contribute to the sum in Eq. (30b).

## V. NUMERICAL METHOD

An approximate analysis of the eigenvalue structure of Eq. (19) can be made by considering scalar models for the operators  $\hat{V}(F^\pm) \sim \pm\omega_b F^\pm$  and  $\hat{C}(F^\pm) \sim -\nu F^\pm$ . Here,  $\nu \equiv \nu_{\text{eff}}$ . If  $dF^\pm/dt$  is retained in Eq. (19), the resulting temporal eigenvalues are  $-\nu \pm i\omega_b$ . Thus, in the low-collision-frequency (high-temperature) regimes of interest, the explicit numerical integration of the underdamped system in Eq. (19) converges only very slowly toward a steady-state solution.<sup>11</sup>

The convergence rate of the explicit temporal integration scheme can be substantially improved by using the energy principle for  $F^\pm$ , Eq. (23b), as the basis for a conjugate gradient minimization method.<sup>18</sup> This method, which generalizes steepest descent techniques, finds the quadratic minimum of  $\dot{S}(F^\pm)$  by successively minimizing  $\dot{S}$  along search directions that are given as appropriate combinations of the local gradients  $g(F^\pm) \equiv MF^\pm - D$ , where  $M = \hat{V}\hat{C}_e^{-1}\hat{V} - \hat{C}$ . Theoretically, the conjugate gradient method should yield the stationary state of  $\dot{S}$ , corresponding to  $g(F^\pm) = 0$ , in at most  $\eta$  iterations, where  $\eta$  is the number of Fourier-Legendre components of  $F^\pm$ . In practice, roundoff errors and large condition numbers for the iteration matrix  $M$  tend to increase this number substantially ( $\sim 5\eta$  to  $10\eta$ ), particularly in the low-collision-frequency regimes where  $\nu \ll \omega_b$ .

Nevertheless, the conjugate gradient scheme is much more efficient at all collision frequencies than explicit temporal integration. One reason for this improved efficiency is that the eigenvalues  $\lambda_M$  of the iteration matrix  $M$  are purely real and damped,  $\lambda_M \approx -(\omega_b^2/\nu + \nu)$ . This

is equivalent to a multiplication of the original system, Eq. (19), by its adjoint operator, with a consequent rotation of the eigenvalue spectrum in the complex plane.

The conjugate gradient method can be accelerated through the application of preconditioning. If an estimate for the inverse of the iteration matrix  $M$  (denoted  $\tilde{M}^{-1}$ ) were available, the resulting approximation for the identity,  $\tilde{M}^{-1}M$ , could be used in the conjugate gradient iteration. (An incomplete Cholesky decomposition<sup>19</sup> of  $M$  is one way to obtain  $\tilde{M}^{-1}$ .)

The main attribute of the conjugate gradient method is the relatively small storage requirement compared with direct matrix inversion techniques. However, the tridiagonal structure of Eq. (26),  $A_{imnl}^Y = 0$ , with respect to the Legendre index  $l$  may be exploited to efficiently invert (with minimal storage) the variational Euler equations for  $F^\pm$ . A block-tridiagonal solver<sup>20</sup> seems to be considerably faster in the low-collision-frequency regimes than the unpreconditioned conjugate gradient method, with a computation time that is nearly independent of  $v/\omega_b$ .

The block-tridiagonal structure of Eq. (26) is apparent since the operators  $Q_{11}^\pm$ , which arise from the streaming and mirror force terms, couple the  $l$ -block to the  $l \pm 1$  blocks. Note that the diagonal of the  $l$ -block row of Eq. (26) involves the collision operator,  $C_l$ . Quite generally, the effective collision frequency increases with  $l$ . Thus, for small values of  $v$ , it is more stable numerically to invert Eq. (26) beginning with the largest value of  $l$  and proceeding backwards to the  $l = 0$  block. This strategy provides better pivots and avoids the

singularity associated with particle and energy conservation in the  $l = 0$  block. The numerical computations discussed in Sec. VI were performed using the block-tridiagonal solution method and a pitch angle scattering form for the collision operator:

$$C_1(f_1) = - \frac{v(K)l(l+1)}{2} f_1 \quad . \quad (31)$$

## VI. NUMERICAL RESULTS

In this section, results for the transport coefficients and distribution function are presented for the  $l = 2$  stellarator configuration analyzed in Ref. 4 using a bounce-averaged Fokker-Planck code. In mks units, the parameters for this device are  $B^{-1} = 0.2[1 + \epsilon_t \cos \theta + \epsilon_h \cos(l\theta - N\zeta)]$ ,  $\epsilon_t = 0.1$ ,  $\epsilon_h = 0.075$ ,  $B_\zeta = 50$ ,  $B_\theta = 0$ ,  $\psi' = 5.0$ ,  $\chi' = 9.0$ ,  $l = 2$ , and  $N = 5$ . The temperature is  $T = 50$  keV. Note that  $\nu = 1.8$  and therefore  $l\nu/N \sim 0.72$  is close to unity. This choice of parameters produces a theoretically predicted resonant enhancement of the transport coefficients in the plateau<sup>6,21</sup> and Pfirsch-Schlüter<sup>7</sup> regimes. These effects are confirmed numerically, indicating that some of the important features of finite  $\nu/N$  can be studied with this model stellarator field. The results of Ref. 4, which were obtained by discarding helical resonances through bounce averaging, may be duplicated with the present code by taking the limit  $N \gg l\nu$ .

The  $B$  contours for this configuration are shown in Fig. 1 for one toroidal field period. Figure 2a shows the variation of  $B$  for one complete toroidal circuit ( $N$  field periods) along the particular magnetic field line  $\theta - \zeta = 0$  when  $N = 5$ ; Fig. 2b shows the same variation, but for  $N = 50$ . For  $N = 5$ , there is no apparent distinction between the helical and the toroidal wells. In contrast, multiple distinct helical wells with short connection lengths appear for  $N = 50$ . For  $N = 50$ , the bounce-averaging procedure in Ref. 4 should be quite accurate.

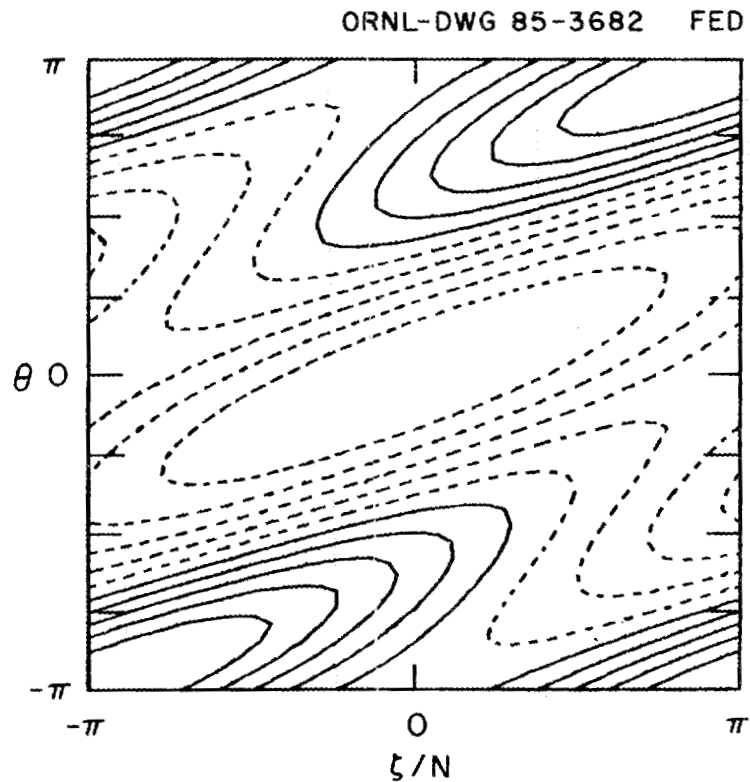


Fig. 1. Contours of  $B$  (magnetic field strength) in one field period for the stellarator configuration  $B = 5[1 - 0.1 \cos \theta - 0.075 \cos(2\theta - N\zeta)]$ . The solid curves correspond to  $B > 5$  and the dashed curves to  $B < 5$ .

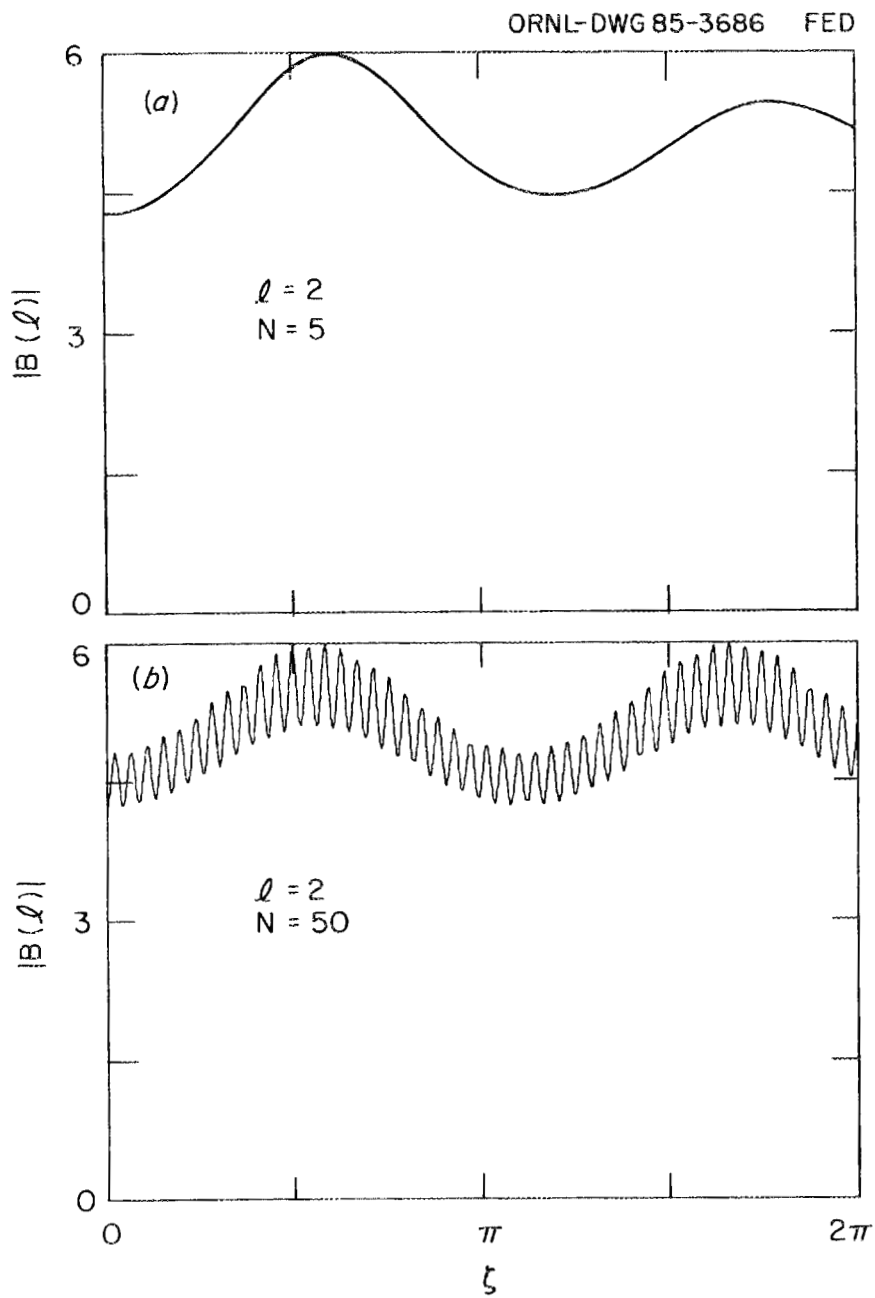


Fig. 2. Variation of  $B$  along the field line  $\theta - \nu\zeta = 0$  for one complete toroidal circuit; (a)  $N = 5$  and (b)  $N = 50$ .

Figure 3 is a plot of the diffusion coefficient  $D_{11}(K=1)$  vs  $\nu_h/\Omega_E$ , where  $\nu_h = \nu(K=1)/(2\epsilon_h)$  is the effective collision frequency for a helically trapped particle and  $\Omega_E = d\Phi_0/d\psi \approx 10^4 \text{ s}^{-1}$  is the electric drift frequency. No dependence on the sign of  $\Omega_E$  has been observed. [This can be shown to be generally valid whenever  $B(\theta, \zeta) = B(-\theta, -\zeta)$  is reflectionally symmetric and when the electric drift dominates the  $\nabla B$  drift.<sup>22</sup>] Numerical results for the two cases,  $N = 5$  (for which helical

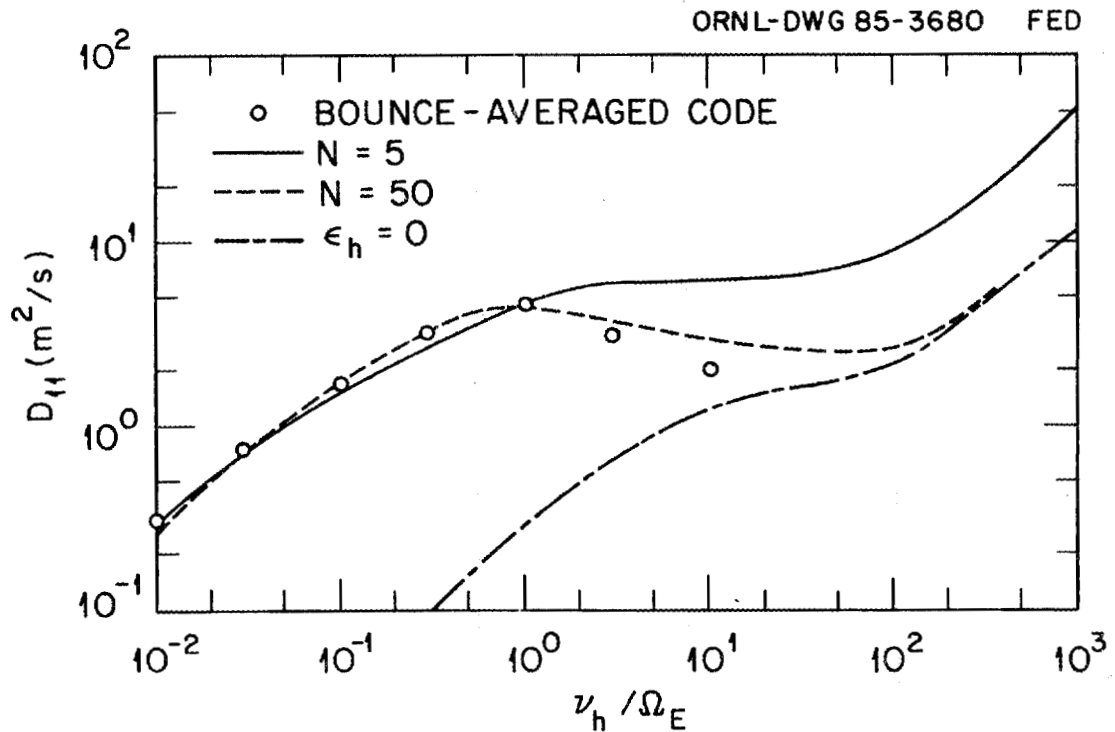


Fig. 3. Diffusion coefficient  $D_{11}$  (in  $\text{m}^2/\text{s}$ ). The solid curve is the result for  $N = 5$ , the dashed curve is for  $N = 50$ , the points are the bounce-averaged results,<sup>4</sup> and the chain-dashed curve represents the equivalent tokamak.

resonances are significant) and  $N = 50$ , are shown. Each point was computed using 7500 components for  $F^+$  and  $F^-$ , which comprised  $L = 80$  pitch angle harmonics,  $M = 12$  poloidal harmonics, and  $N = 8$  toroidal harmonics. This required about 50 s of cpu time on the CRAY-2. (Fewer harmonics than this were sufficient to obtain converged results for the transport coefficients at the higher collision frequencies.) For comparison, the  $N \rightarrow \infty$  (bounce-averaged) results<sup>4</sup> are presented (open points). In addition, an  $\epsilon_h = 0$  tokamak equivalent (with  $\iota = 1.8$ ) is shown as a benchmark. There is close agreement between the  $N = 50$  results and the bounce-averaged values of  $D_{11}$  for  $v_h/\Omega_E < 1$ . For  $v_h/\Omega_E > 1$  and  $N = 5$ , the observed resonant enhancement of diffusion over the tokamak value is in good agreement with theoretical predictions:

$$\frac{D_{11}}{D_{11}^{\text{tok}}} = \begin{cases} 1 + \frac{\tau_{1N}}{\tau_{10}} \left(\frac{\epsilon_h}{\epsilon_t}\right)^2 \approx 3.9 \text{ (plateau) ,} \\ 1 + \left(\frac{\tau_{1N}}{\tau_{10}}\right)^2 \left(\frac{\epsilon_h}{\epsilon_t}\right)^2 \approx 4.7 \text{ (Pfirsch-Schlüter) .} \end{cases} \quad (32)$$

Here,  $\tau_{mn} = |m - n/\iota|^{-1}$  is the normalized resonant transit time. For  $N = 50$ , the helical resonance is reduced in the plateau regime and nearly vanishes in the collisional regime. [This agrees with the analytic formulas in Eq. (32).] The discrepancy between the results for  $N = 50$  and the bounce-averaged code in the banana-plateau transition region,  $v_h/\Omega_E \approx 10$ , may be related to the finite difference representation used in Ref. 4 for the region of pitch angle space outside the helical well.

The contours of the toroidally averaged distribution function,  $\int f d\zeta$ , are depicted in Figs. 4 and 5 for  $N = 5$  and  $N = 50$ , respectively, in the helically trapped ("superbanana") regime  $v_h/\Omega_E = 0.01$ . Solid contours represent an excess of particles ( $f_1 > 0$ ) and dashed ones a depletion ( $f_1 < 0$ ). The dominant features of these figures for  $N = 50$ , including the steep gradients in the vicinity of the boundary between trapped and circulating particles ( $|\cos \alpha| = (2\varepsilon_h)^{1/2} = 0.39$ ) and the hill and valley structures centered at  $\theta = \pm\pi$  and  $\theta = 0$ , respectively, are in qualitative agreement with the bounce-averaged results.<sup>4</sup> Note that the contours for both  $v_{\parallel} > 0$  and  $v_{\parallel} < 0$  are continuous, which is in contrast to the near discontinuity for counter-streaming velocities obtained in Ref. 4 at the helical trapping boundary. Contours for the more collisional regime  $v_h/\Omega_E = 10$  (banana-plateau transition) are shown in Figs. 6 and 7. For this case, the gradients are much weaker at the helical trapping transition, and the hill-valley structure has shifted by  $\Delta\theta = \pm\pi/2$ , in agreement with Ref. 4.

The dependence of the diffusion coefficient  $D_{11}$  on the electric drift is shown in Fig. 8. The solid curve represents the universal scaling  $D\Omega_E = h(v_h/\Omega_E)$  valid in the limit  $N \rightarrow \infty$ . It was obtained for  $N = 50$  and values of  $eaE_{\rho}/T$  in the range 0.5 to 4.0. For  $N = 5$ , there are significant deviations from the universal curve. (Note that the case with  $eaE_{\rho}/T = 2$  is closest to the universal scaling and is also the case for which Fig. 3 was obtained.) For values of  $v_h/\Omega_E < 0.1$  far from the  $1/v$  transition,  $D_{11}$  obeys an approximate power law:

$$D \sim \left( \frac{v_h}{\Omega_E} \right)^P . \quad (33)$$

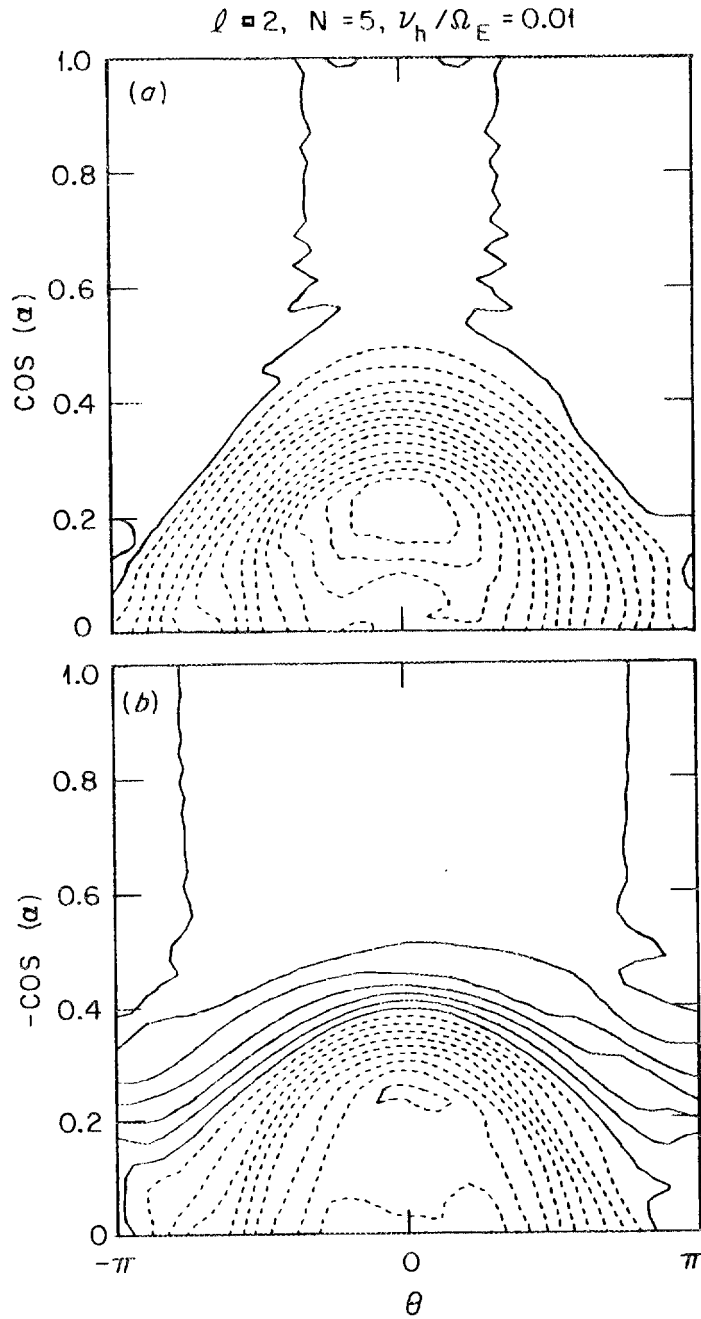


Fig. 4. The contours of  $\int f_1 d\zeta$  for  $\nu_h/\Omega_E = 0.01$  and  $N = 5$ . (a)  $v_{\parallel} > 0$ , (b)  $v_{\parallel} < 0$ . Solid curves represent an excess of particles ( $f_1 > 0$ ) and dashed ones a depletion ( $f_1 < 0$ ).

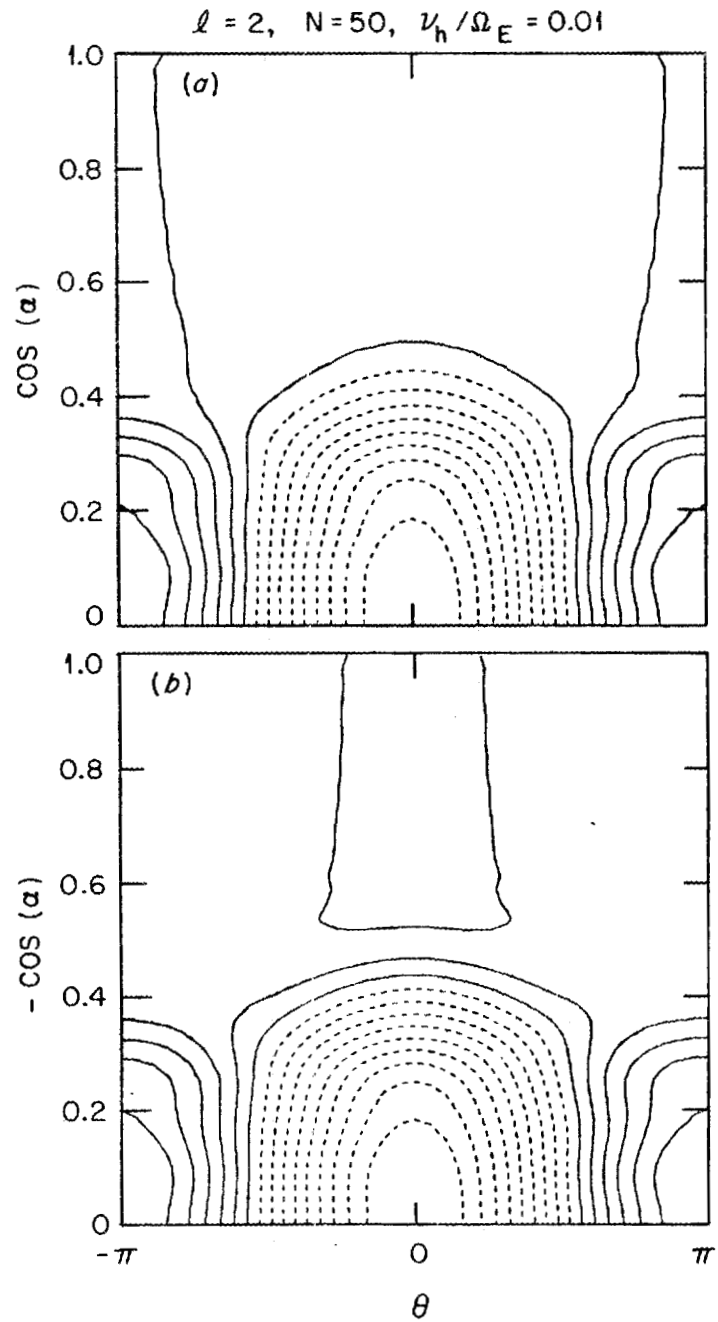


Fig. 5. The contours of  $\int f_1 d\zeta$  for  $\nu_h / \Omega_E = 0.01$  and  $N = 50$ . (a)  $v_{||} > 0$ , (b)  $v_{||} < 0$ .

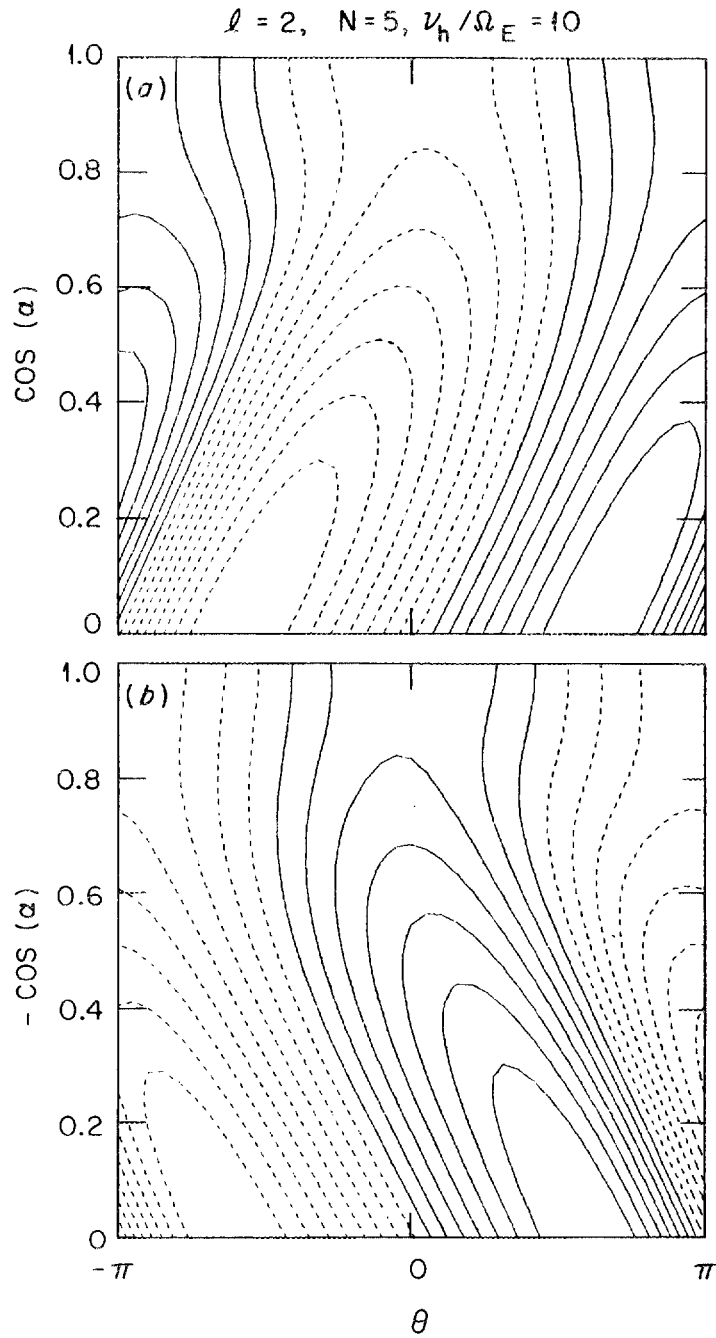


Fig. 6. The contours of  $\int f_1 d\zeta$  for  $\nu_h / \Omega_E = 10$  and  $N = 5$ . (a)  $v_{\parallel} > 0$ , (b)  $v_{\parallel} < 0$ .

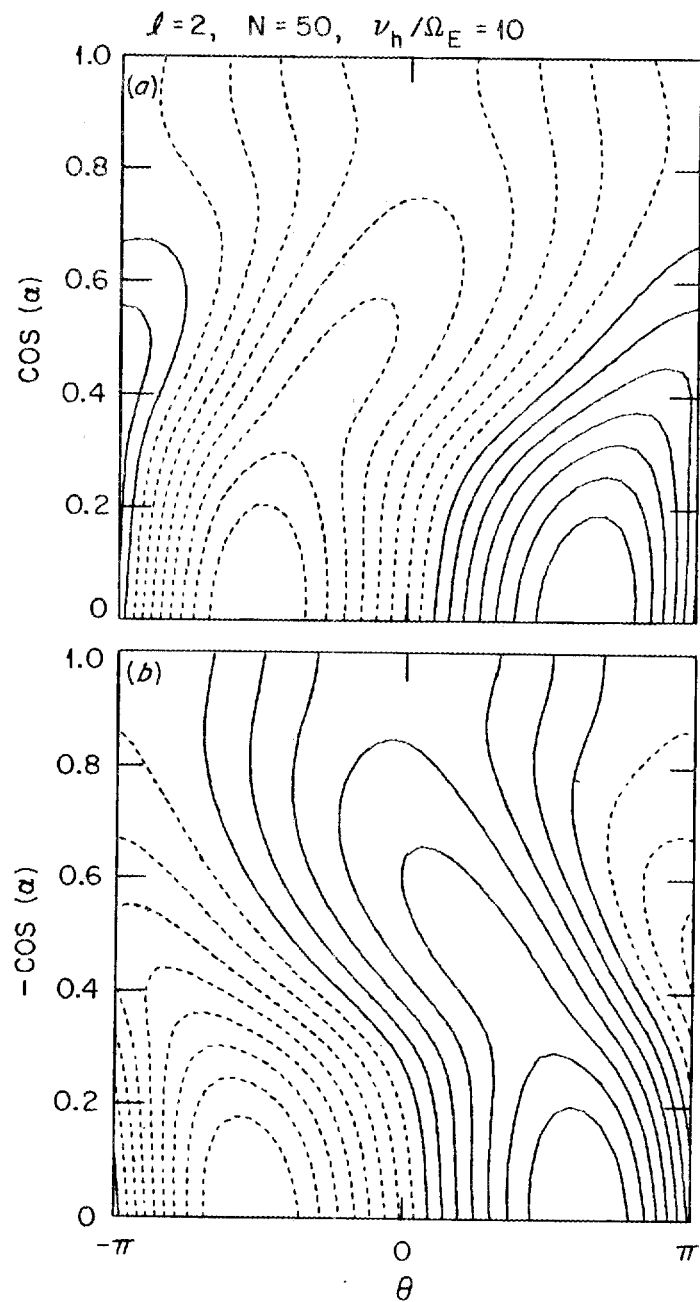


Fig. 7. The contours of  $\int f_1 d\zeta$  for  $\nu_h / \Omega_E = 10$  and  $N = 50$ . (a)  $v_{\parallel} > 0$ , (b)  $v_{\parallel} < 0$ .

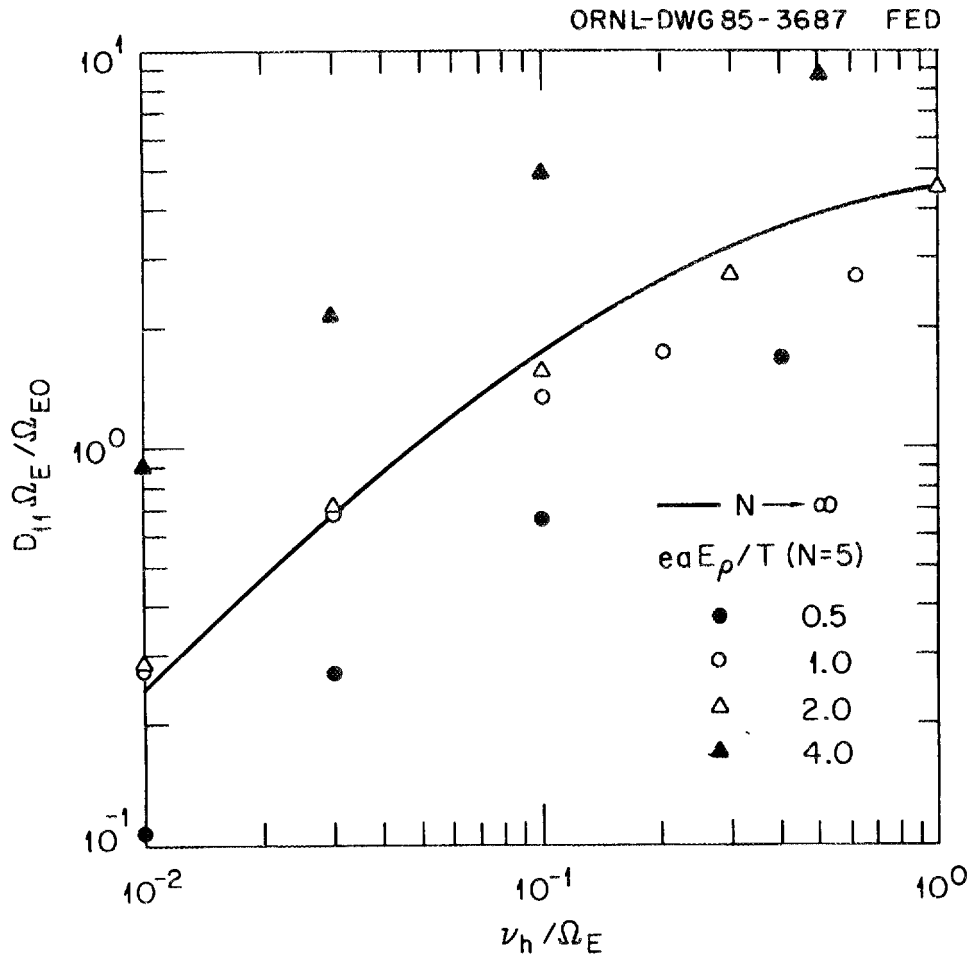


Fig. 8. Value of  $D_{11} \Omega_E / \Omega_{E0}$  vs  $\nu_h / \Omega_E$ , where  $\Omega_{E0} = \Omega_E (eaE_\rho / T = 2)$ . The solid curve is for  $N = 50$ .

For  $N = 50$ ,  $p \approx 0.93$  is close to the scaling predicted from collisionless detrapping processes<sup>1,2,3</sup> alone ( $p = 1$ ). In contrast, for  $N = 5$ , the value  $p \approx 0.82$  lies between the values predicted from collisionless detrapping and collisional boundary layer effects<sup>3</sup> ( $p = 0.75$ ). These results suggest that the transport in configurations without well-defined local helical wells may be a complex combination

of both collisional scattering and collisionless trapping processes. The electric drift scaling for  $N = 5$  indicates the importance of transition particles in such systems.

The Ware-pinch coefficient  $D_{13}$  is plotted in Fig. 9 where it is normalized to the equivalent tokamak value. For  $N = 5$ ,  $D_{13}$  never exceeds the tokamak value, thus indicating the relatively small

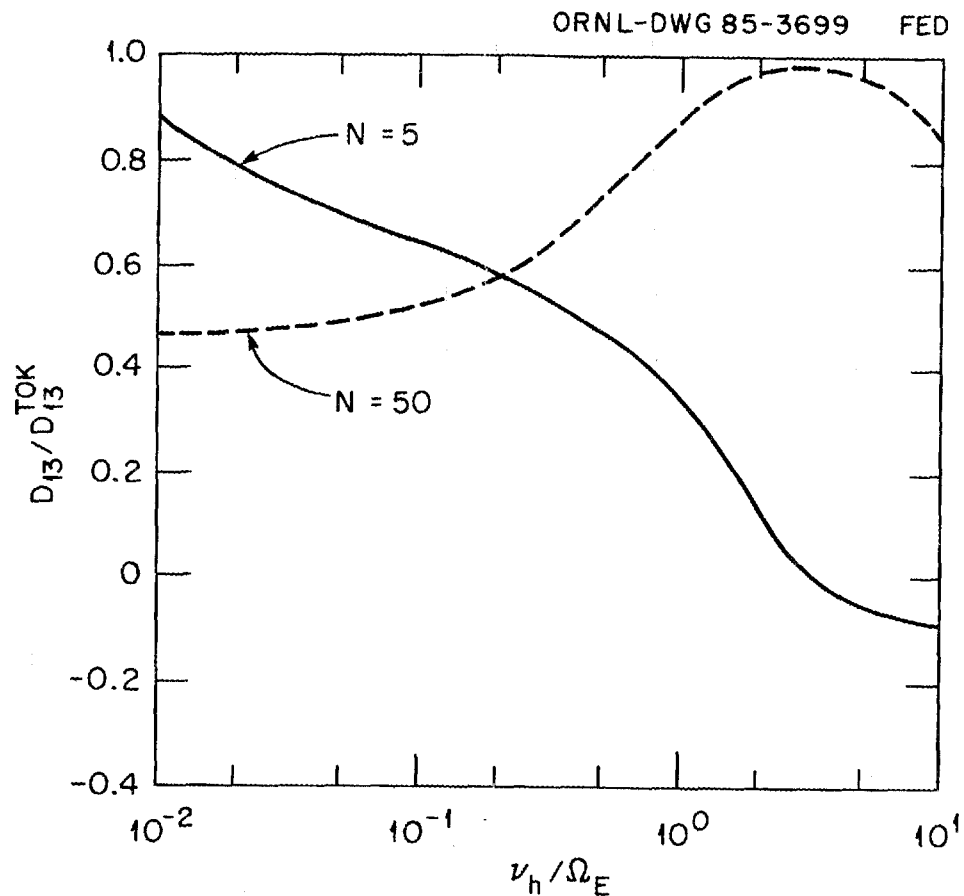


Fig. 9. The Ware-pinch coefficient  $D_{13}$  normalized to the equivalent tokamak value. The solid curve is for  $N = 5$ , and the dashed curve is for  $N = 50$ .

bootstrap current ( $\propto D_{31} = D_{13}$ ) in this device. The sign change in  $D_{13}$  is associated with the change in the relative importance of helical vs toroidal effects in determining the bootstrap current.<sup>21</sup>

## VII. CONCLUSIONS

The derivation of a variational principle for computing local transport coefficients for 3-D plasma confinement configurations has been presented. A numerical method has been developed for solving the Euler equations that determine the particle distribution function in Fourier-Legendre space. Application to a stellarator model with a finite value of  $1/N$  has shown the importance of helical resonances and transition particle effects for radial transport and bootstrap current. Studies of Heliac configurations, for which bounce-averaging methods are inapplicable, are currently in progress.<sup>24</sup>

## ACKNOWLEDGMENTS

The authors are grateful to W. N. G. Hitchon and H. E. Mynick for stimulating conversations concerning the relationship of the present work with Ref. 4.

This research was sponsored by the Office of Fusion Energy, U. S. Department of Energy, under Contract No. DE-AC05-84OR21400 with Martin Marietta Energy Systems, Inc.

## REFERENCES

- <sup>1</sup>K. C. Shaing, J. A. Rome, and R. H. Fowler, *Phys. Fluids* 27, 1 (1984).
- <sup>2</sup>H. E. Mynick, *Phys. Fluids* 26, 2609 (1983).
- <sup>3</sup>L. M. Kovrizhnykh, *Nucl. Fusion* 24, 851 (1984).
- <sup>4</sup>H. E. Mynick and W. N. G. Hitchon, A Bounce-Averaged Fokker Planck Code for Stellarator Transport, PPPL-2235, Princeton University, 1985.
- <sup>5</sup>K. C. Shaing and J. D. Callen, *Phys. Fluids* 26, 3315 (1983).
- <sup>6</sup>M. Coronado-Gallardo, Ph.D. Thesis, Technischen Universität, Munich (1984).
- <sup>7</sup>A. H. Boozer, *Phys. Fluids* 24, 1999 (1981).
- <sup>8</sup>A. H. Boozer and G. Kuo-Petravic, *Phys. Fluids* 24, 851 (1981).
- <sup>9</sup>R. E. Potok, P. A. Politzer, and L. M. Lidsky, *Phys. Rev. Lett.* 45, 1328 (1980).
- <sup>10</sup>J. S. Tolliver, *Phys. Fluids* 28, 1083 (1985); W. N. G. Hitchon, C. D. Beidler, H. E. Mynick, and J. L. Shohet, *Nucl. Fusion* 25, 105 (1985).
- <sup>11</sup>C. O. Beasley, Jr., J. E. McCune, H. K. Meier, and W. I. Van Rij, *Plasma Phys.* 19, 593 (1977).
- <sup>12</sup>R. D. Hazeltine, *Plasma Phys.* 15, 77 (1973).
- <sup>13</sup>W. I. Van Rij, H. K. Meier, C. O. Beasley, Jr., and J. E. McCune, *Plasma Phys.* 19, 135 (1977).
- <sup>14</sup>D. V. Sivukhin, in Reviews of Plasma Physics, edited by M. A. Leontovich (Consultants Bureau, New York, 1965), Vol. 1, p. 97.
- <sup>15</sup>S. P. Hirshman and J. C. Whitson, *Phys. Fluids* 26, 3553 (1983).
- <sup>16</sup>A. A. Galeev, R. Z. Sagdeev, H. P. Furth, and M. N. Rosenbluth, *Phys. Rev. Lett.* 22, 511 (1969).

- <sup>17</sup>E. A. Frieman, *Phys. Fluids* 13, 490 (1970).
- <sup>18</sup>M. R. Hestenes and E. Stiefel, *J. Res. Natl. Bur. Stand.* 49, 409 (1952).
- <sup>19</sup>D. S. Kershaw, *J. Comput. Phys.* 26, 43 (1978).
- <sup>20</sup>A. C. Hindmarsh, Solution of Block-Tridiagonal Systems of Linear Algebraic Equations, UCID-30150, Lawrence Livermore Laboratory, February 1977.
- <sup>21</sup>K. C. Shaing, S. P. Hirshman, and J. D. Callen, *Phys. Fluids* 29, in press (1986).
- <sup>22</sup>S. P. Hirshman, K. C. Shaing and W. I. van Rij, Consequences of Time-Reversal Symmetry for the Electric Field Scaling of Transport in Stellarators, ORNL/TM-9908, Oak Ridge National Laboratory, in preparation.
- <sup>23</sup>A. A. Galeev and R. Z. Sagdeev, *Sov. Phys. Usp.* 14, 810 (1969).
- <sup>24</sup>E. Solano, J. A. Rome, and J. F. Lyon, *Bull. Am. Phys. Soc.* 30, 1575 (Abstract 7S9) (1985).

## INTERNAL DISTRIBUTION

- |                         |  |
|-------------------------|--|
| 1. S. E. Attenberger    | 22. J. A. Rome                                       |
| 2. D. B. Batchelor      | 23. M. J. Saltmarsh                                  |
| 3. C. O. Beasley        | 24-28. K. C. Shaing                                  |
| 4. B. A. Carreras       | 29. D. A. Spong                                      |
| 5. L. A. Charlton       | 30. J. S. Tolliver                                   |
| 6. E. C. Crume, Jr.     | 31. J. C. Whitson                                    |
| 7. R. A. Dory           | 32. J. Sheffield                                     |
| 8. R. H. Fowler         | 33-34. Laboratory Records Department                 |
| 9-13. S. P. Hirshman    | 35. Laboratory Records, ORNL-RC                      |
| 14. J. A. Holmes        | 36. Document Reference Section                       |
| 15. W. A. Houlberg      | 37. Central Research Library                         |
| 16. H. C. Howe          | 38. Fusion Energy Division<br>Library                |
| 17. D. K. Lee           | 39-40. Fusion Energy Division<br>Publications Office |
| 18. J. F. Lyon          | 41. ORNL Patent Office                               |
| 19. M. Murakami         |  |
| 20. Y-K. M. Peng        |  |
| 21. E. Rodriguez-Solano |  |

## EXTERNAL DISTRIBUTION

42. Office of the Assistant Manager for Energy Research and Development, Department of Energy, Oak Ridge Operations Office, P. O. Box E, Oak Ridge, TN 37830
43. J. D. Callen, Department of Nuclear Engineering, University of Wisconsin, Madison, WI 53706
44. R. W. Conn, Department of Chemical, Nuclear, and Thermal Engineering, University of California, Los Angeles, CA 90024
45. S. O. Dean, Director, Fusion Energy Development, Science Applications International Corporation, Gaithersburg, MD 20760

46. H. K. Forsen, Bechtel Group, Inc., Research Engineering, P. O. Box 3965, San Francisco, CA 94105
47. J. R. Gilleland, GA Technologies, Inc., Fusion and Advanced Technology, P.O. Box 85608, San Diego, CA 92138
48. R. W. Gould, Department of Applied Physics, California Institute of Technology, Pasadena, CA 91125
49. R. A. Gross, Plasma Research Laboratory, Columbia University, New York, NY 10027
50. D. M. Meade, Princeton Plasma Physics Laboratory, P.O. Box 451, Princeton, NJ 08544
51. W. M. Stacey, School of Nuclear Engineering, Georgia Institute of Technology, Atlanta, GA 30332
52. D. Steiner, Rensselaer Polytechnic Institute, Troy, NY 12181
53. R. Varma, Physical Research Laboratory, Navrangpura, Ahmedabad 380009, India
54. Bibliothek, Max-Planck Institut fur Plasmaphysik, D-8046 Garching bei Munchen, Federal Republic of Germany
55. Bibliothek, Institut fur Plasmaphysik, KFA, Postfach 1913, D-5170 Julich, Federal Republic of Germany
56. Bibliotheque, Centre des Recherches en Physique des Plasmas, 21 Avenue des Bains, 1007 Lausanne, Switzerland
57. Bibliotheque, CEN/Cadarache, Departement de Recherches sur la Fusion Controlee, 13108 Saint-Paul-lez-Durance, France
58. Documentation S.I.G.N., Departement de la Physique du Plasma et de la Fusion Controlee, Centre d'Etudes Nucleaires, B.P. 85, Centre du Tri, 38081 Grenoble, France
59. Library, Culham Laboratory, UKAEA, Abingdon, Oxfordshire, OX14 3DB, England
60. Library, FOM-Instituut voor Plasma-Fysica, Rijnhuizen, Edisonbaan 14, 3439 MN Nieuwegein, The Netherlands
61. Library, Institute of Plasma Physics, Nagoya University, Nagoya, Japan
62. Library, International Centre for Theoretical Physics, Trieste, Italy
63. Library, Laboratorio Gas Ionizzati, CP 56, I-00044 Frascati, Rome, Italy

64. Library, Plasma Physics Laboratory, Kyoto University, Gokasho, Uji, Kyoto, Japan
65. Plasma Research Laboratory, Australian National University, P.O. Box 4, Canberra, A.C.T. 2000, Australia
66. Thermonuclear Library, Japan Atomic Energy Research Institute, Tokai, Naka, Ibaraki, Japan
67. G. A. Eliseev, I. V. Kurchatov Institute of Atomic Energy, P. O. Box 3402, 123182 Moscow, U.S.S.R.
68. V. A. Glukhikh, Scientific-Research Institute of Electro-Physical Apparatus, 188631 Leningrad, U.S.S.R.
69. I. Shpigel, Lebedev Physical Institute, Leninsky Prospect 53, 117924 Moscow, U.S.S.R.
70. D. D. Ryutov, Institute of Nuclear Physics, Siberian Branch of the Academy of Sciences of the U.S.S.R., Sovetskaya St. 5, 630090 Novosibirsk, U.S.S.R.
71. V. T. Tolok, Kharkov Physical-Technical Institute, Academical St. 1, 310108 Kharkov, U.S.S.R.
72. Library, Academia Sinica, P.O. Box 3908, Beijing, China (PRC)
73. J. F. Clarke, Associate Director for Fusion Energy, Office of Energy Research, ER-50, Germantown, U.S. Department of Energy, Washington, DC 20545
74. W. Sadowski, Fusion Theory and Computer Services Branch, Office of Fusion Energy, Office of Energy Research, ER-541, Germantown, U.S. Department of Energy, Washington, DC 20545
75. N. A. Davies, Office of the Associate Director, Office of Fusion Energy, Office of Energy Research, ER-51, Germantown, U.S. Department of Energy, Washington, DC 20545
76. E. Oktay, Division of Confinement Systems, Office of Fusion Energy, Office of Energy Research, ER-55, Germantown, U.S. Department of Energy, Washington, DC 20545
77. M. N. Rosenbluth, Institute for Fusion Studies, University of Texas, RLM 11.218, Austin, TX 78712
78. Theory Department Read File, c/o D. W. Ross, Institute for Fusion Studies, University of Texas, Austin, TX 78712
79. Theory Department Read File, c/o R. C. Davidson, Director, Plasma Fusion Center, NW 16-202, Massachusetts Institute of Technology, Cambridge, MA 02139

80. Theory Department Read File, c/o F. W. Perkins, Princeton Plasma Physics Laboratory, P.O. Box 451, Princeton, NJ 08544
81. Theory Department Read File, c/o L. Kovrizhnykh, Lebedev Institute of Physics, Academy of Sciences, 53 Leninsky Prospect, 117924 Moscow, U.S.S.R.
82. Theory Department Read File, c/o B. B. Kadomtsev, I. V. Kurchatov Institute of Atomic Energy, P.O. Box 3402, 123182 Moscow, U.S.S.R.
83. Theory Department Read File, c/o T. Kamimura, Institute of Plasma Physics, Nagoya University, Nagoya, Japan
84. Theory Department Read File, c/o C. Mercier, Euratom-CEA, Service des Recherches sur la Fusion Controlee, Fontenay-aux-Roses (Seine), France
85. Theory Department Read File, c/o T. E. Stringer, JET Joint Undertaking, Culham Laboratory, Abingdon, Oxfordshire OX14 3DB, England
86. Theory Department Read File, c/o K. Roberts, Culham Laboratory, Abingdon, Oxfordshire OX14 3DB, England
87. Theory Department Read File, c/o D. Biskamp, Max-Planck-Institut fur Plasmaphysik, D-8046 Garching bei Munchen, Federal Republic of Germany
88. Theory Department Read File, c/o T. Takeda, Japan Atomic Energy Research Institute, Tokai, Naka, Ibaraki, Japan
89. Theory Department Read File, c/o C. S. Liu, GA Technologies, Inc., P.O. Box 81608, San Diego, CA 92138
90. Theory Department Read File, c/o L. D. Pearlstein, Lawrence Livermore National Laboratory, P.O. Box 808, Livermore, CA 94550
91. Theory Department Read File, c/o R. Gerwin, CTR Division, Los Alamos National Laboratory, P.O. Box 1663, Los Alamos, NM 87545
92. R. E. Mickens, Department of Physics, Atlanta University, Atlanta, GA 30314
93. G. Bateman, Princeton Plasma Physics Laboratory, P.O. Box 451, Princeton, NJ 08544
94. I. Bernstein, Yale University, New Haven, CT 06520
95. A. Bers, 38-260, Massachusetts Institute of Technology, Cambridge, MA 02139
96. O. Betancourt, Courant Institute of Mathematical Sciences, New York University, 251 Mercer Street, New York, NY 10012

97. A. Bhattacharjee, Columbia University, New York, NY 10027
98. H. H. Chen, Physics Department, University of Maryland, College Park, MD 20742
99. L. Chen, Princeton Plasma Physics Laboratory, P.O. Box 451, Princeton, NJ 08544
100. J. Cordey, Culham Laboratory, UKAEA Research Group, Abingdon, Oxfordshire OX14 3DB, England
101. J. DeLucia, Princeton Plasma Physics Laboratory, P.O. Box 451, Princeton, NJ 08544
102. P. Garabedian, Courant Institute of Mathematical Sciences, New York University, 251 Mercer Street, New York, NY 10012
103. A. Glasser, Los Alamos National Laboratory, Los Alamos, NM 87545
104. H. Goedbloed, Plasma Fusion Center, NW 16-243, Massachusetts Institute of Technology, Cambridge, MA 02139
105. H. Grad, Magnets-Fluid Dynamics Division, Courant Institute of Mathematical Sciences, New York University, 251 Mercer Street, New York, NY 10012
106. J. M. Greene, GA Technologies, Inc., San Diego, CA 92138
107. L. Hall, L-630, Lawrence Livermore National Laboratory, P.O. Box 5511, Livermore, CA 94550
108. L. Ibanez, Courant Institute of Mathematical Sciences, New York University, 251 Mercer Street, New York, NY 10012
109. S. C. Jardin, Princeton Plasma Physics Laboratory, P.O. Box 451, Princeton, NJ 08544
110. W. Kerner, Courant Institute of Mathematical Sciences, New York University, 251 Mercer Street, New York, NY 10012
111. L. L. Lao, T0-512, GA Technologies, Inc., San Diego, CA 92138
112. K. M. Liang, Los Alamos National Laboratory, Los Alamos, NM 87545
113. R. McCall, Princeton Plasma Physics Laboratory, P.O. Box 451, Princeton, NJ 08544
114. B. Miner, Science Applications International Corporation, 1710 Goodridge Drive, McLean, VA 22102
115. R. W. Moses, MS 642, Los Alamos National Laboratory, Los Alamos, NM 87545
116. H. Mynick, ECE Department, Princeton Plasma Physics Laboratory, Princeton, NJ 08544
117. J. Nuhrenberg, Max Planck Institute for Plasma Physics, D-8046 Garching, Federal Republic of Germany

118. N. Pomphrey, Princeton Plasma Physics Laboratory, P.O. Box 451, Princeton, NJ 08544
119. A. Riedel, Courant Institute of Mathematical Sciences, New York University, 251 Mercer Street, New York, NY 10012
120. P. H. Rutherford, Princeton Plasma Physics Laboratory, P.O. Box 451, Princeton, NJ 08544
121. A. G. Sgro, Los Alamos National Laboratory, Los Alamos, NM 87545
122. A. Schluter, Max Planck Institute for Plasma Physics, D-8046 Garching, Federal Republic of Germany
123. U. Schwenn, Max Planck Institute for Plasma Physics, D-8046 Garching, Federal Republic of Germany
124. V. D. Shafranov, I. V. Kurchatov Institute of Atomic Energy, P.O. Box 3042, 123182 Moscow, U.S.S.R.
125. J. L. Shohet, Stellarator-Torsatron Laboratory, University of Wisconsin, Madison, WI 53706
126. A. M. M. Todd, Grumman Aerospace Corporation, 105 College Road East, Princeton, NJ 08540
127. Y. M. Treve, 125 San Rafael Avenue, Santa Barbara, CA 93109
128. J. W. Van Dam, Institute for Fusion Studies, RLM.222, University of Texas, Austin, TX 78712
129. H. Weitzner, Courant Institute of Mathematical Sciences, New York University, 251 Mercer Street, New York, NY 10012
130. J. C. Wiley, Institute for Fusion Studies, RLM 11.222, University of Texas, Austin, TX 78712
- 131-284. Given distribution according to TIC-4500, Magnetic Fusion Energy (Distribution Category UC-20 g: Theoretical Plasma Physics)